Development of Synchrotron-Based X-Ray Scatter Projection Imaging

Christopher Dydula[1], George Belev[2] and Paul C. Johns[1]

[1] Dept. Physics, Carleton University, Ottawa [2] Canadian Light Source, Saskatoon

Abstract

In medical x-ray imaging a major challenge is to obtain adequate soft tissue contrast. The goal of our research is to develop a high soft-tissue contrast x-ray technique based on the detection of low-angle scattered photons. Scattered photons comprise up to 90% of the radiation downstream of the patient and can provide information in addition to that of the transmitted primary x rays. In particular, the cross section for coherent x-ray scattering, the basis of x-ray diffraction, varies with angle and photon energy in a material-specific manner, even for amorphous materials, and thus it can provide good soft tissue contrast. At the photon energies of medical radiology coherent scatter is a minority of all photon interactions, but its forward nature at these energies makes it relatively easy to detect. For example, in abdominal radiography coherent single scatter is 10% of the total scatter and 26% of the primary fluence.

We are developing x-ray scatter imaging at the BioMedical Imaging & Therapy (BMIT) facility of the Canadian Light Source (CLS) synchrotron in Saskatoon, Canada. The BMIT facility provides an excellent development environment with the availability of monoenergetic x-ray beams, flat-panel x-ray imagers and automated sample positioning stages. The best images are obtained using step-and-shoot scanning with a pencil beam and area detector to capture sequentially the scatter pattern for each primary beam location on the sample. Primary x-ray transmission is recorded simultaneously using photodiodes. Our beam energy is 33.2 keV and the pencil beam area is about 2.7 mm^2. The technological challenge is to acquire the scatter data in a reasonable time. Our aim is to acquire images on a time scale similar to that of nuclear medicine, e.g., under 15 minutes. Geometries using multiple pencil beams producing partially-overlapping scatter patterns reduce acquisition time but increase the complexity due to the need for a disentangling algorithm to extract the data. Continuous sample motion, rather than step-and-shoot, also reduces acquisition time at the expense of introducing motion blur and is the subject of our latest investigation. Our recent work with plastic phantoms and animal tissues is described.

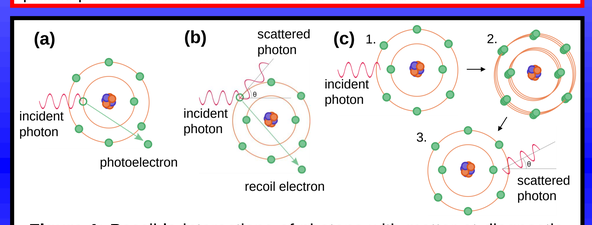

Figure 1: Possible interactions of photons with matter at diagnostic energies. **(a)** Photoelectric effect – photon disappears; sensitive to atomic number. **(b)** Incoherent (Compton) scattering – photon scattered; sensitive to electron density. **(c)** Coherent (Rayleigh) scattering – photon scattered; sensitive to chemical composition.

1 – Introduction

At the energy range of diagnostic radiology, 15 - 150 keV, a photon can interact with matter in three different ways (**Figure 1**) or it may not interact at all [1]. **Figure 2** shows the cross sections for each of these three interactions.

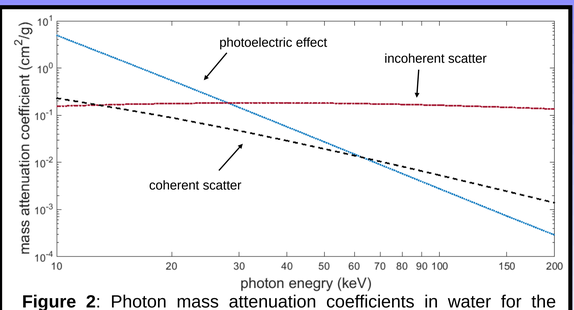

Figure 2: Photon mass attenuation coefficients in water for the possible interaction mechanisms in the diagnostic energy range [2].

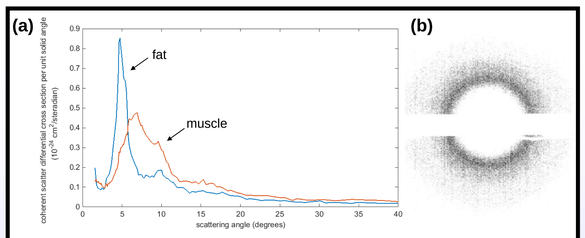

Figure 3: **(a)** Probability of coherent scatter vs scattering angle for 33.2 keV photons [3]. The angular dependence of the scattering cross section is shown for two soft tissues; the differences can be exploited to provide good soft tissue contrast. **(b)** Scatter pattern detected when shining a pencil beam through fat.

2 – Objective

Although coherent scatter is a minority of photon interactions (**Figure 2**), its angular dependence is highly forward peaked (**Figure 3a**). Up to 15% of photons reaching the detector in projection imaging are coherent scatter photons [1] but these have traditionally gone unused, despite coherent scatter's sensitivity to chemical composition. The goal is therefore to develop projection imaging utilizing coherently scattered photons, focusing on minimizing the time to acquire an image. Medical applications are in breast, prostate and neurological imaging. Security applications are in baggage screening [4].

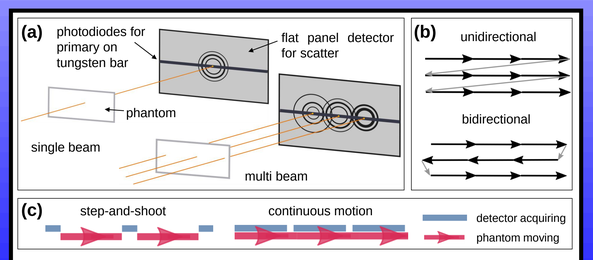

Figure 4: **(a)** General setup of scatter projection imaging using one vs multiple pencil beams. **(b)** The phantom can be raster scanned with pencil beams while moving in one or in both directions. **(c)** Acquisition method can be step-and-shoot or continuous motion.

3 – Methods

We are developing a scatter projection imaging prototype at the BMIT facility at CLS [5] (**Figure 4**). The phantom is translated on a stage to expose each section of it to a 2.7 mm^2 pencil beam at 33.2 keV. The x-ray photons in the beam are scattered according to the coherent and incoherent scattering cross sections of the material located at that section of the phantom (**Figure 3a**). The coherently scattered photons create a Laue pattern behind the phantom (**Figure 3b**) whose radial intensity corresponds to the angular dependence of the scattering cross section. This pattern is captured using a Hamamatsu C9252DK-14 flat panel detector. The pattern is converted to a radial profile, which has a shape similar to the scattering cross section, and is then integrated over an angular range, selected to maximize contrast between particular materials, to generate the pixel value. The primary beam is measured simultaneously with a photodiode.

The simplest acquisition scheme is using a single pencil beam with unidirectional step-and-shoot scanning. Acquisition can be sped up using multiple pencil beams simultaneously. This creates overlapping scatter patterns at the detector which are then disentangled using a maximum-likelihood expectation-maximization algorithm [6]. Continuous motion also speeds up acquisition but introduces motion blur. For step-and-shoot, data pixels are collected in a hexagonal array, spaced 1.68 mm horizontally, 1.455 mm vertically and detector acquisition time is 66 μs per pixel. For continuous motion, it is a rectangular array with 1 mm horizontal spacing and 100 μs acquisition per pixel. The stage velocity is 10 mm/s (motor limit). Data acquisition is automated by controlling the hardware with a LabVIEW program. The primary and scatter data are analyzed using MATLAB.

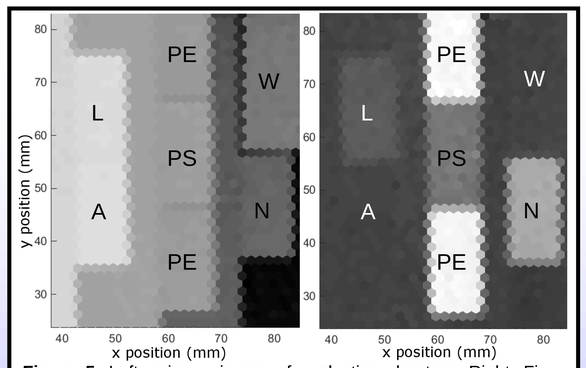

Figure 5: Left: primary image of a plastics phantom. Right: Five-beam scatter image of the same phantom, radial profiles integrated over 6° - 7°. Components of the phantom are labeled: L: lexan, A: acrylic, PE: polyethylene, PS: polystyrene, W: water, N: nylon. Plastics which appear identical in the primary image become distinguishable in the scatter image.

Figure 6: Pork phantom. Left: front side, facing x-ray source. Right: back side, facing detector. The plastic container is filled with saline.

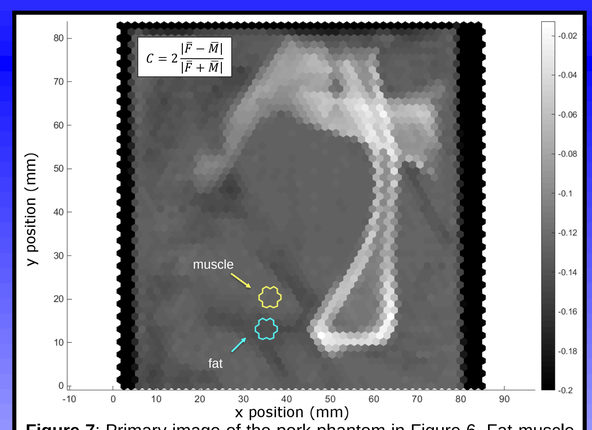

Figure 7: Primary image of the pork phantom in Figure 6. Fat-muscle contrast is 0.10 ± 0.01. Insert: formula for calculating contrast; $\bar{F}$ is the mean of the outlined fat pixel values, $\bar{M}$ is the muscle pixel mean.

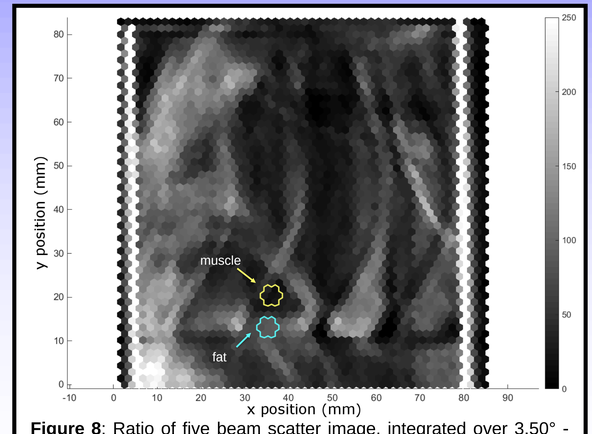

Figure 8: Ratio of five beam scatter image, integrated over 3.50° - 5.57°, to primary image in Figure 7. Fat–muscle contrast is 1.2 ± 0.2.

4 – Results and Discussion

Figure 5 shows the primary and scatter images for a phantom of plastic blocks. The contrasts between lexan and acrylic and between polyethylene and polystyrene are visibly higher in the scatter image.

Figure 6 is a pork phantom imaged at the hardware limit for speed using step-and-shoot acquisition with five beams. **Figure 7** is the primary image. **Figure 8** is the scatter image divided by the primary image to correct for attenuation. Fat-muscle contrast has a tenfold improvement in the second image. Using multiple beams speeds up acquisition but introduces ghosting artefacts of strongly attenuating structures, such as bone, due to limitations in the scatter-pattern disentanglement algorithm.

Figure 9 shows preliminary results for an even faster acquisition technique using continuous motion. Additional artefacts from motion blur and from blur correction techniques affect the image.

The ongoing development of an x-ray scatter imaging prototype is summarized in **Figure 10**. As of the fourth iteration, acquiring an 8 cm x 8 cm image takes less than 15 minutes, on the time scale of nuclear medicine.

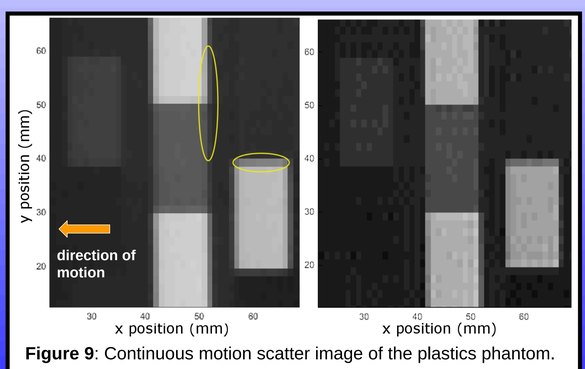

Figure 9: Continuous motion scatter image of the plastics phantom.

Left: Measured pixel values. Outlined are aperture and motion blur artefacts. The blurred measured data are given as $B = R * A * M$, where R = true pixel value, A = aperture point spread function (PSF), M = motion blur PSF and $*$ denotes convolution. The true pixel value at row j and column k is computed using deconvolution:

$$R[j,k] = \sum_m \sum_n B[n,m] \cdot w\,[k-n, j-m],$$

where the weights w are inverse Fourier integrals depending on the models for A and M. We model A and M as rectangle functions and use a 23 x 23 convolution kernel.

Right: Result of current blur deconvolution algorithm. Blurring at edges is reduced somewhat but other periodic artefacts arise.

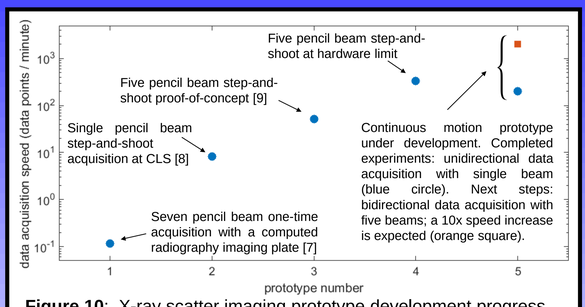

Figure 10: X-ray scatter imaging prototype development progress.

5 – Conclusions

Utilizing coherently scattered photons can enhance the contrast between materials such as soft tissues or plastics in x-ray projection images. Prototype development has focused on decreasing image acquisition time which is now on the order of a nuclear medicine scan. However, techniques for improving acquisition speed also introduce image artefacts such as ghosting and motion blur. Future work will be to correct these artefacts while further increasing acquisition speed.

Acknowledgements

This work was supported by the Natural Sciences and Engineering Research Council of Canada (NSERC). The first author thanks the CLS Graduate and Post-Doctoral Student Travel Support Program for assistance. Research described in this presentation was performed at the BMIT facility at the Canadian Light Source, which is funded by the Canada Foundation for Innovation, NSERC, the National Research Council Canada, the Canadian Institutes of Health Research, the Government of Saskatchewan, Western Economic Diversification Canada, and the University of Saskatchewan.

References

[1] P. C. Johns and M. J. Yaffe, "Coherent scatter in diagnostic radiology," *Med. Phys.*, vol. 10, no. 1, pp. 40-50, 1983. [doi: 10.1118/1.595443].

[2] M. J. Berger, J. H. Hubbell, S. M. Seltzer, J. Chang, J. S. Coursey, R. Sukumar, D. S. Zucker, and K. Olsen. (2010), *XCOM: Photon Cross Section Database* (version 1.5) [Online]. Available: http://physics.nist.gov/xcom [27-May-2016]. NIST, Gaithersburg, MD.

[3] B. W. King, K. A. Landheer, and P. C. Johns, "X-ray coherent scattering form factors of tissues, water and plastics using energy dispersion," *Phys. Med. Biol.*, vol. 56, no. 14, pp. 4377-4397, 2011. [doi: 10.1088/0031-9155/56/14/010].

[4] G. Harding et al., "X-ray diffraction imaging with the Multiple Inverse Fan Beam topology: Principles, performance and potential for security screening," *Appl. Radiat. Isotopes*, vol. 70, no. 7, pp. 1228-1237, 2012. [doi: 10.1016/j.apradiso.2011.12.015].

[5] T. W. Wysokinski, D. Chapman, G. Adams, M. Renier, P. Suortti, and W. Thomlinson, "Beamlines of the biomedical imaging and therapy facility at the Canadian Light Source - part 3," *Nucl. Instrum. Meth. A*, vol. 775, pp. 1-4, 2015. [doi: 10.1016/j.nima.2014.11.088].

[6] K. A. Landheer and P. C. Johns, "Coherent x-ray scatter projection imaging using an array of monoenergetic pencil beams," in *Chem., Biol., Radiol., Nucl., and Explosives (CBRNE) Sensing XIII*, vol. 8358 of *Proc. SPIE*, pp. 672-681, 2012. [doi: 10.1117/12.918666].

[7] M. Nisar and P. C. Johns, "Coherent scatter x-ray imaging of plastic/water phantoms," in *Photonics North 2004: Photonic Applications in Astron., Biomed., Imaging, Mater. Processing, and Education*, vol. 5578 of *Proc. SPIE*, pp. 445-453, 2004. [doi: 10.1117/12.567128].

[8] K. A. Landheer and P. C. Johns, "Coherent scatter ring integration imaging," poster presented at Joint AAPM/COMP Meeting, Vancouver, BC, Jul. 31 – Aug. 4, 2011. Abstract: *Med. Phys.*, vol. 38, no. 6, p. 3439, 2011. [doi: 10.1118/1.3611761].

[9] K. A. Landheer and P. C. Johns, "Synchrotron-based coherent scatter x-ray projection imaging using an array of monoenergetic pencil beams," *Rev. Sci. Instrum.*, vol. 83, no. 9, pp. 095114-1 – 095114-7, 2012. [doi: 10.1063/1.4754124].

Contribution ID: 1230 - CAP - Ottawa, Ontario - 2016 June 13-17